since 1961

Baltica

BALTICA Volume 32 Number 1 June 2019: 63–77
https://doi.org/10.5200/baltica.2019.1.6

Seismic shocks, periglacial conditions and glaciotectonics as causes of the deformation of a Pleistocene meandering river succession in central Lithuania

Małgorzata Pisarska-Jamroży, Szymon Belzyt, Albertas Bitinas, Asta Jusienė, Barbara Woronko

Pisarska-Jamroży, M., Belzyt S., Bitinas A., Jusienė A., Woronko B. 2019. Seismic shocks, periglacial conditions and glaciotectonics as causes of the deformation of a Pleistocene meandering river succession in central Lithuania. *Baltica, 32 (1),* 63–77. Vilnius. ISSN 0067-3064.

Manuscript submitted 11 February 2019 / Accepted 08 May 2019 / Published online 20 June 2019

Abstract. An extraordinary variation of plastic and brittle deformation structures with periglacial, glaciotectonic and seismic features was observed within the unconsolidated, upper Pleistocene meandering river succession in the Slinkis outcrop in central Lithuania. Among these deformations, the following structures were described: (1) ice-wedge casts in the lower part of the sedimentary succession, linked to periglacial processes, (2) soft-sediment deformation structures, such as load structures (load casts, pseudonodules), flame structures and water/sediment-escape structures, all trapped in clearly defined layers in the upper part of the sedimentary succession, which are related to the propagation of seismic waves, and (3) faults occurring throughout the sedimentary succession, which are associated with glaciotectonic processes. To our knowledge, this is the first description and analysis of the combined presence of such a diverse range of deformation features caused by three trigger mechanisms in a meandering fluvial sedimentary succession.

Keywords: *soft-sediment deformation structures; brittle deformations; seismite; periglacial features; glaciotectonic deformations; liquefaction; meandering river deposits*

✉ *Małgorzata Pisarska-Jamroży (pisanka@amu.edu.pl, szymon.belzyt@amu.edu.pl) Institute of Geology, Adam Mickiewicz University, B. Krygowskiego 12, 61-680 Poznań, Poland; Albertas Bitinas (albertas.bitinas@gamtc.lt) Nature Research Centre, Akademijos 2, LT-08412 Vilnius, Lithuania; Asta Jusienė (asta.jusiene@lgt.lt) Lithuanian Geological Survey, S. Konarskio 35, Vilnius LT-03123, Lithuania; Barbara Woronko (bworonko@uw.edu.pl) Warsaw University, Faculty of Geology, Żwirki i Wigury 93, 02-089 Warsaw, Poland*

INTRODUCTION

Different types of soft-deformation structures occur most commonly in fine-grained unconsolidated siliciclastic sediments and develop shortly after deposition at a very early diagenetic stage. Most cases are observed in fine-grained lacustrine sediments (Alfaro *et al.* 1997; Gladkov *et al*. 2016), glaciolacustrine sediments (Schwan, Van Loon 1979; Goździk, Van Loon 2007; Brooks 2018; Pisarska-Jamroży *et al*. 2018, 2019), and mass-movement sediments (Alsop, Marco 2011). These types of deformation structure have also been described from aeolian (Bryant *et al.* 2016) and fluvial deposits (Rana *et al*. 2016), but more rarely. In contrast, brittle and periglacial deformation structures can be found in all types of sediments, regardless of their granulometric composition (Evans *et al*. 2006; Ruszczyńska-Szenajch, Trzciński 2009; Pisarska-Jamroży, Zieliński 2012; Weckwerth, Pisarska-Jamroży 2015; Woronko *et al.* 2018).

The range of processes and agents that can induce soft-sediment deformation structures is wide, and for this reason, the reconstruction of their origin is often problematic. Furthermore, the overprinting of simultaneously or successively acting factors/triggers and their overlapping traces in the sedimentary record (Van Loon, Brodzikowski 1987; Van Loon 2009; Pisarska-Jamroży 2013; Belzyt, Pisarska-Jamroży 2017) can complicate the interpretation of the origin of the deformation structures. In glacigenic sediments, deformation structures are most commonly ascribed to periglacial and glacitectonic processes; such periglacial and glacitectonic features occurring during the Weichselian glaciation have been widely described across the territory of Lithuania (e.g. Aleksa, Bitinas 2000; Aber, Ber 2007; Baltrūnas *et al.* 2007, 2010), as well as other previously glaciated areas south of the Baltic Sea (e.g. Dzierżek, Stańczuk 2006; Ewertowski 2009; Pedersen 2014; Gehrmann, Harding, 2018). It is possible that glacigenic sediments could be deformed during periods of ice-front fluctuations under the influence of external factors such as the passage of shock waves resulting from seismic activity. It was found in the past few decades that the deformation of Quaternary sediments could be induced by the rather frequent earthquakes triggered by Earth's crustal rebound (termed GIA = glacial isostatic adjustment) in front of the ice sheet (e.g. Johnston 1987; Muir-Wood 2000; Stewart *et al.* 2000; Grollimund, Zoback 2001; Steffen, Wu 2011; Brandes *et al.* 2012; Steffen *et al.* 2014; Brandes *et al.* 2015; Van Loon *et al.* 2016). Such seismic waves may result in the creation of seismites, these being layers with soft-sediment deformation structures of seismic origin (Hoffmann, Reicherter 2012; Brandes *et al.* 2012; Van Loon, Pisarska-Jamroży 2014; Pisarska-Jamroży *et al.* 2018; Pisarska-Jamroży, Woźniak 2019). GIA has mainly been thought to occur during deglaciation (e.g. Bitinas, Lazauskienė 2011; Bitinas 2012; Hoffmann, Reicherter 2012; Van Loon, Pisarska-Jamroży 2014; Brandes *et al.* 2015; Van Loon *et al.* 2016; Druzhinina *et al.* 2017; Pisarska-Jamroży, Woźniak 2019); however, recent studies suggest that GIA may also take place in front of advancing ice sheet (see Brandes *et al.* 2011; Pisarska-Jamroży *et al.* 2018), probably during ice-sheet movements.

It is also worth noting that presently seismic waves are commonly emitted from various sources, including iceberg calving, basal motion, glacier hydraulics and englacial fracture development (e.g. Podolskiy, Walter 2016 and references therein). They can all trigger glacial earthquakes, which are detected within a distance of tens of hundreds of kilometres (Nettles, Ekström 2010), but until now, only Phillips *et al.* (2018) have noted the presence of soft-sediment deformation structures caused by glacial earthquakes in subglacial conditions.

A highly unusual discovery was recently made in the Slinkis outcrop in central Lithuania, where three groups of deformation structures caused by three different trigger mechanisms were found to co-occur in a single 5 m-high sedimentary succession (Fig. 1). The main goal of the study is to unravel the development of these deformation structures by determining the most probable trigger mechanisms and characterizing the deposition and deformation conditions. In addition, the present study aims to indicate the features of each of the three groups of deformation structure which generally could be used in the recognition of trigger mechanisms based on the lithological and deformational features of the sediments.

GEOLOGICAL SETTING

The Slinkis outcrop is situated in the western part of central Lithuania (Figs. 1, 2), and is assigned to the Nevėžis Plain (Guobytė 1990). The relief and sediment cover of the study area were formed at the very end of the Last Glaciation (Upper Weichselian) and during the Holocene (Jusienė 2004). The hummocky morainic plain (till plain; at the altitude of about 60–65 metres a.s.l.) was deposited during Last Glacial deglaciation. The depressions of the hummocky morainic plain consist of layers of very fine-grained sand, silt/clay, or rarely, sand with gravel a few metres thick, which have been deposited from meltwaters. During the Holocene, the morainic plain was eroded by waters of the Nemunas River and its tributaries, and deep valleys were formed (Fig. 2).

The Slinkis outcrop, located in the area of the Nemunas and Dubysa River confluence (Fig. 1), is situated in the lower course of the Dubysa River, the right tributary of the Nemunas River, 3 km to the N of the Nemunas River valley. The investigated section is outcropping along the steeply incised river valley (Fig. 3A). The lateral extent of the outcrop is limited by the talus deposits totally covering the adjacent slopes of the valley (Fig. 3).

MATERIALS AND METHODS

The textural and structural features of the sediments were described using a lithofacies code following Miall (1977), as modified by Zieliński and Pisarska-Jamroży (2012). A two-level subdivision of sediments was used, including a distinction between lithofacies and their associations. Two lithofacies associations were distinguished (lower and upper) and will be referred to as unit A and unit B, respectively, for the present study (see Fig. 3B). The mesoscale structural features (orientation of the fault planes, the axial planes of the folds, as well as the fault offsets) were measured. Their results were projected and mean orientation calculated using Stereonet 10 software (lower hemisphere projection). The grain size of the sediments in the Slinkis outcrop is indicated according to the Udden-Wentworth scale. Two samples

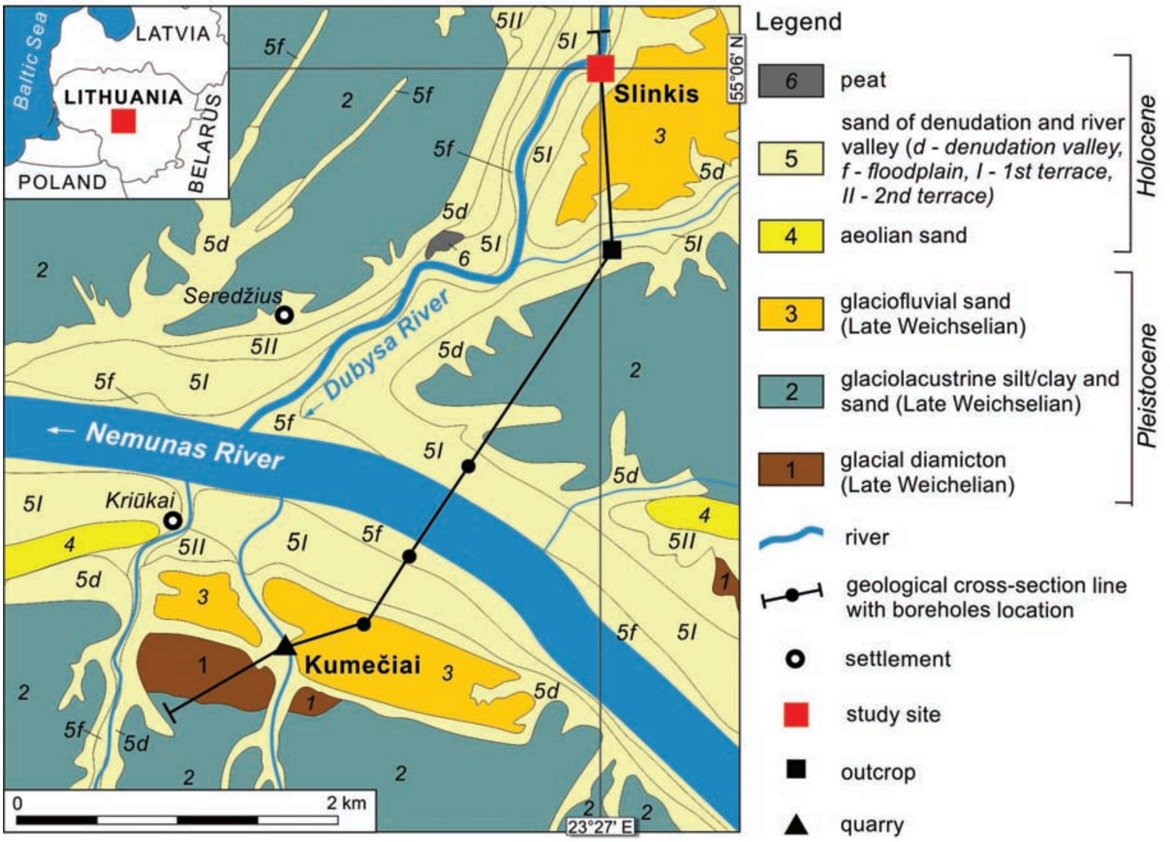

Fig. 1 Geological map of the study area with the Slinkis outcrop location (modified after Jusienė 2004)

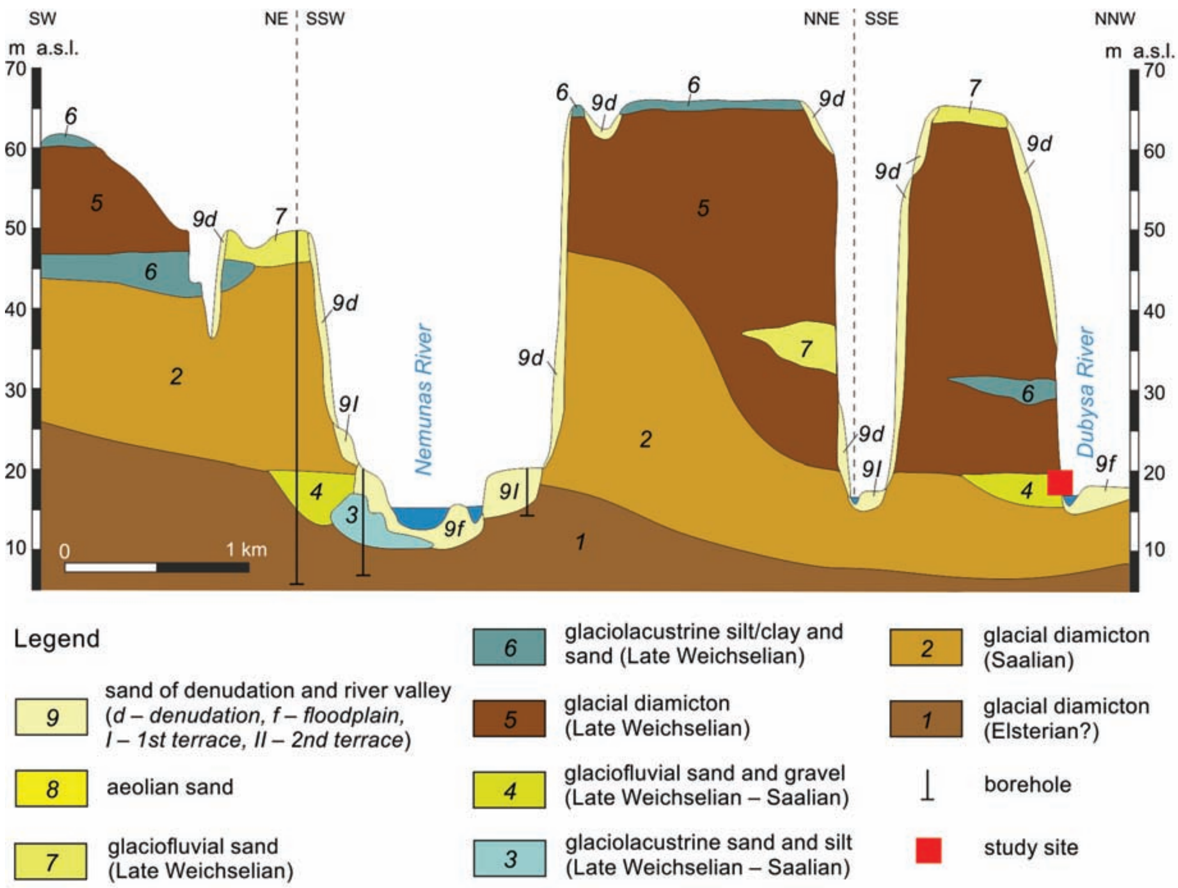

Fig. 2 Geological cross-section through the study area. For location see Fig. 1

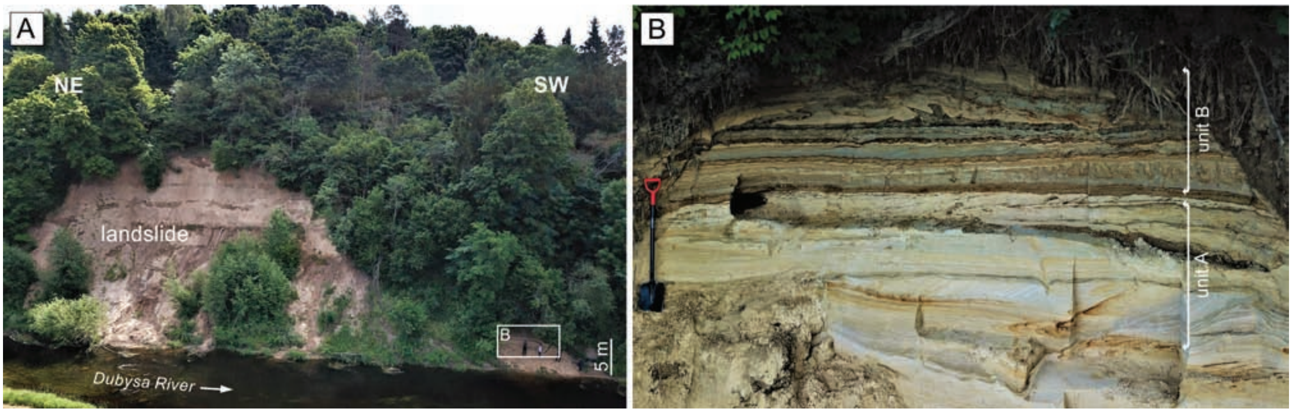

Fig. 3 General view of the Slinkis outcrop. **A:** Slope of the Dubysa River valley with Holocene-age landslide which exposed ca. 20-metre-thick glacial diamicton. **B:** Sedimentary succession in the Slinkis outcrop with distinguished two sedimentary units A and B

for optically stimulated luminescence (OSL) dating were collected from cross-stratified sandy deposits of the upper part of unit A. The measurements were performed at the GADAM Gliwice Luminescence Laboratory in Poland using the standard multi-grain aliquots method. Equivalent doses of samples were determined using the single-aliquot regenerative-dose (SAR) protocol. In addition, the results of pollen analysis, obtained during geological mapping carried out by Lithuanian Geological Survey at a scale of 1:50,000, were also taken into consideration (Jusienė 2004).

SEDIMENTARY SUCCESSION IN THE SLINKIS OUTCROP

The sedimentary succession description

The sedimentary succession in the Slinkis outcrop was observed in a 5 m-high and 6.5 m-wide outcrop orientated NE-SW and located along the left bank of the Dubysa River (Fig. 3). The sedimentary succession comprise two sedimentary units: lower A and upper B (Fig. 4A–C). The boundary between units A and B is erosional. Unit B is covered by a 0.5–1.2 m-thick massive glacial diamicton (=till, lithofacies Dm; Fig. 4C); however, the total thickness of this diamiction reaches almost 20 m in the immediate vicinity of the section (Fig. 3A). The deformation structures recognised within both units were described and interpreted in the corresponding chapter.

Unit A consists mainly of sandy sediments: planar-, low angle-, trough cross-stratified and ripple-cross laminated sands with admixtures of silts (lithofacies Sp, Sl, St and Sr, respectively; Fig. 4D–F). The excavated part of the unit A is at least 2.3-m thick and the thickness of individual lithofacies varies from a few up to 50 cm. The lower and upper boundaries of the lithofacies are mostly sharp, and the upper boundaries of the lithofacies often show erosional features. The lithofacies have a lenticular shape and their lateral extent varies from 2.3 to 4.6 m. The grain size distribution along the whole unit A shows a slight upward fining. OSL dating results indicate that the upper part of unit A was deposited approximately 22.4 ± 1.2 and 22.6 ± 1.4 ka (GdTL–2862 and GdTL–2863, respectively; Fig. 4C).

Unit B is more fine-grained than unit A. Its overall thickness reaches 55–65 cm, while the thickness of individual lithofacies varies from 7 to 22 cm (Fig. 4B, C). The lithofacies extend along the whole width of the outcrop. Unit B is composed of ripple cross-laminated and wavy-laminated silt, ripple cross-laminated sandy silt and fine-grained sand for lithofacies Fr, Fw, FSr, Sr, respectively; lithofacies Sp comprise planar cross-stratified sand, and lithofacies Fm massive silts; furthermore, deformed sandy silt and silt lithofacies also occur (FSd and Fd lithofacies, respectively; see details in in the corresponding subchapter below). In the upper part of unit B were detected pollen (Fig. 4B) of *Botrychium, Selaginella selaginoides, Lycopodium selago* and *Betula nana* (Jusienė 2004).

The sedimentary succession interpretation

In the lower unit A, a fractional meandering succession of the compound bar (Fig. 4D) and a laterally accreted point bar typically occurring in meandering rivers were recognized (Fig. 4E). The lower part of the point bar was, most probably, situated below the average river water level, while the upper part was covered by waters only during flood events (see Zieliński 2014). Floods caused erosion of the upper part of the point bar (platform or superplatform, up to 40 cm), resulting in the development of a chute (see Fig. 4E). Furthermore, the microdelt forms of the chute bar (from 5 up to 12 centimetres) were accumulated (Fig. 4F).

Above unit A, the presence of fine-grained sediments (unit B) suggests accumulation at the distal

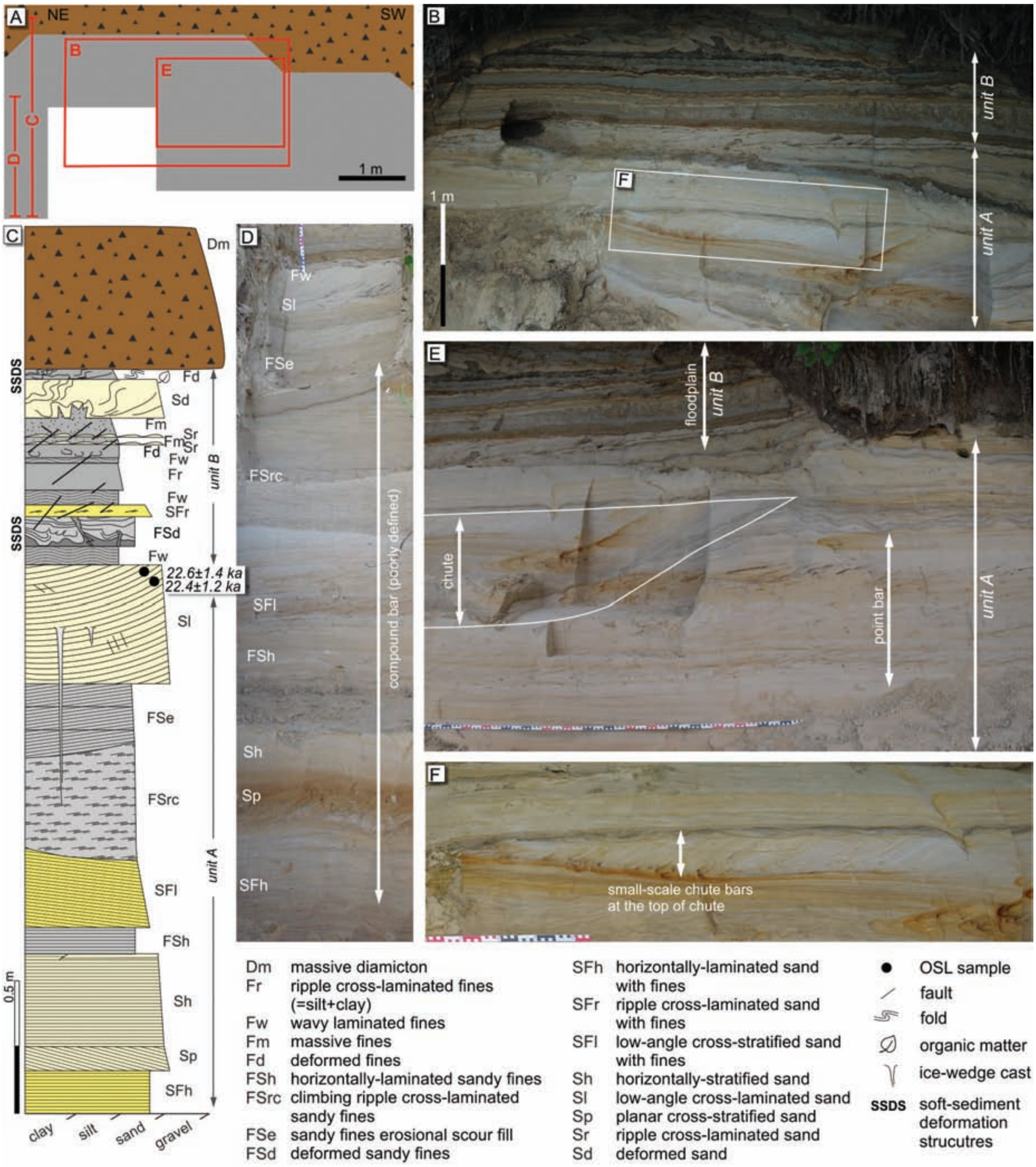

Fig. 4 Sedimentary succession at the Slinkis outcrop. **A:** Schematic view of the outcropping sediments. **B:** Two sedimentary units A and B. **C:** Sedimentary log with two units A and B overlain by glacial diamicton and distribution of deformation structures: ice-wedge casts, soft-sediment deformation structures and faults. **D:** Meandering river succession of a compound bar. **E–F:** Close-up view of meandering river sediments (point bars, chute bars, floodplain deposits) within unit A

part of the floodplain of the meandering river. The ripple cross-laminated sediments (lithofacies Fr, SFr, Sr) were deposited as flow-regime bedforms from slowly moving, small-volume inflows that used to interrupt phases of water stagnation and suspension fallout (lithofacies Fw, Fm). Due to successive phases of deposition from suspension in water and the erosion processes occurring during higher stages of the waters, the shape of visible layers is more lenticular or trough-like than sheet-like.

Both sedimentary units A and B in the Slinkis outcrop were deposited in a meandering fluvial system during a cold climate, as indicated by *inter alia* the periglacial tundra type of pollen found in the uppermost part of unit B (see Jusienė 2004; Borisova 2005). Cold-stage fluvial systems typically demonstrate a braided channel pattern with wide and shallow channels; however, the fluvial system in the Slinkis outcrop succession is more characteristic of meandering river sediments with imprints of periglacial features and tundra vegetation pollen. This cold meandering system existed in front of the advancing Weichselian ice sheet. Sandy glaciofluvial sediments supplied this meandering river, thus increasing its aggradational potential. This issue is a part of general discussion on changes in fluvial temperate and cold systems, as well as a lag in the reaction of the fluvial system to climatic change (see Krzyszkowski 1991, 1996; Vandenberghe *et al.* 1994; Huisink 2000; Gibbard, Lewin 2002; Vandenberghe 2008; Zieliński *et al.* 2016).

DEFORMATION STRUCTURES IN THE SLINKIS OUTCROP DEPOSITIONAL SUCCESSION

Three groups of deformation structures were recognized in the Slinkis outcrop: (1) cryostructures in unit A, (2) soft-sediment deformation structures (abbr. SSDS) in the lower part of unit B, and (3) faults in units A and B.

The cryostructures in unit A

Description

Two wedge-like structures (1.2 m-long and 5 cm-long) were recognised in unit A (Fig. 5A–C). Both cut the chute bar deposits, with the larger also cutting the overlying low-angle cross-stratified sands of the point bar (Fig. 4F at right side). The width of the larger wedge-like structure in the base ran from a few millimetres (thickness of 5–10 veins) to 15–20 cm in the uppermost part. This wedge-like structure is divided into two parts: a lower part beginning in planar cross-laminated sands with admixtures of silt, and an upper one running from low-angle cross-stratified sands (Fig. 5C). The smaller wedge-like structure was found at the same level as the upper part of the larger wedge-like structure (Fig. 5B).

The orientation of the larger wedge-like structure plane axis slightly varies with depth, dipping generally to the S-SW with a nearly vertical (82–85°) angle (Fig. 5C). The general trend of the plane axis azimuth is perpendicular to the outcrop extent (E-W, NW-SE).

Interpretation

The wedge-like structures were interpreted as epigenetic/syngenetic ice-wedge casts which grow upwards in response to surface aggradation. In the larger ice-wedge cast, the presence of two growth stages, described as lower and upper (see previous subchapter), implies its rejuvenation. During the first stage, 5–10 narrow ice veins, 0.5 cm wide and more than 100 cm deep, were formed in a thermal-contraction

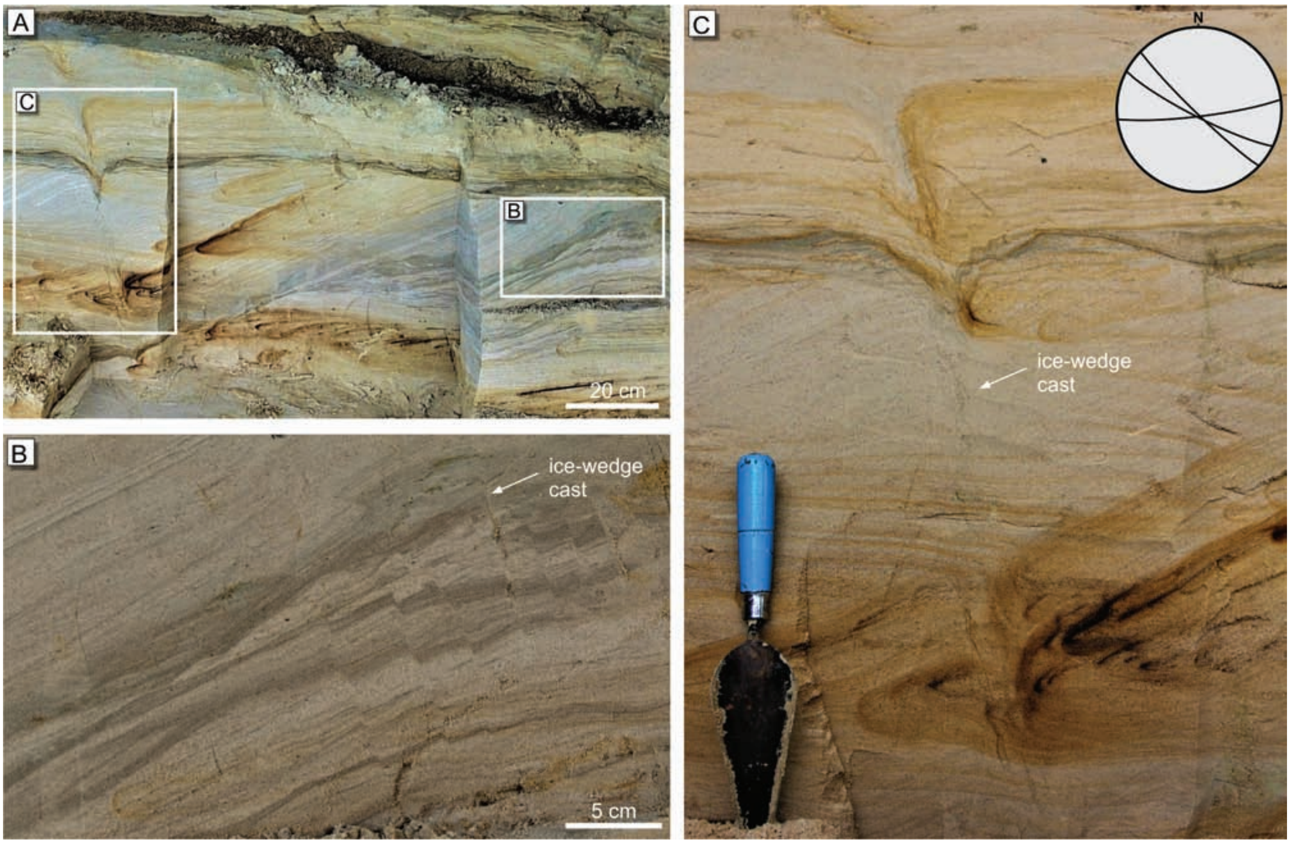

Fig. 5 Periglacially induced deformation structures in the Slinkis outcrop. **A:** Distribution of ice-wedge casts within sediments of unit A. **B:** Small ice-wedge cast with a set of syndepositional small-scale faults. **C:** Ice-wedge cast cutting chute bar deposits and stereographic projection of ice-wedge cast orientation measurements

crack. The veins were opened in approximately the same place for 5–10 years. The width and depth of these ice veins was approximately the same throughout their length. Some of the ice veins are infilled by massive grey silty clay, probably from the overlying active layer. Near the palaeosurface, the lower part of the ice-wedge cast widens, reaching 15–20 cm. The general narrowness of the wedge indicates that the sedimentation rate was relatively high and ice-vein accretion was low (see French 2007); however, the process of aggradation appears to have stopped for a few years between the two stages of ice-wedge cast development. A distinct widening towards the top of the ice-wedge cast in the first stage of formation suggest that this structure is epigenetic in nature (French, Goździk 1988). During the second stage, the upper part of the bigger ice-wedge cast was opened in the same place as the lower one and it was the beginning of syngenetic growth. The presence of downwarps probably indicates that the fissure originally penetrated permafrost, and that voids were filled with sediments from the fissure walls as the ice melted (French, Goździk 1988). The smaller ice-wedge cast was developed at the same time as the upper part of the larger ice-wedge cast and it is epigenetic.

The soft-sediment deformation structures in unit B

Description

Two separated layers with numerous SSDS were recognised in the lower part of unit B (Figs. 4C, 6). Both deformed layers, *viz.* the lower deformed layer and the upper deformed layer, are interbedded with 20 cm-thick undeformed sediments of a similar grain size as these deformed layers. The brittle deformation structures which accompany the SSDS, often cutting them, are described in the subchapter below.

Lower deformed level

The thickness of the lower layer with the SSDS (lithofacies FSd) ranges from 15 to 35 cm (Fig. 6A). The base boundary of the deformed layer is sharp while the top boundary has erosional features. The SSDS within lithofacies FSd are distributed more or less regularly along the visible part of the deformed layer (Fig. 6B). Silty sediment-escape structures, i.e. detached and undetached sandy load casts, have been recognised (Fig. 6A–H). A set of narrow, slender water/sediment-escape structures measuring up to 12 cm long, intrude into the overlying ripple cross-laminated sandy deposits branching out in the uppermost part (Fig. 6B–D). Most water/sediment-escape structures have a sharp top edge (Fig. 6B, E–H). Sometimes, vertical and subvertical pillars and channels of water/sediment-escape structures, measuring up to 5 cm long and less than 0.5 cm wide, caused deformation of underlying laminae in the downwards direction (Fig. 6E). The load casts have variable sizes of up to 14 cm length and 10 cm width, and vary in shape from elongated to rounded. In most cases, the internal laminae of the load casts are not curved, but straight and perpendicular to the edge of the cast, demonstrating only slight local bending in the proximity of the load cast edge (Fig. 6B–E). The boundaries between the water/sediment-escape structures and the loading structures are sharp in most cases (Fig. 6D), but sometimes a mixture of sandy and silty sediments creates a narrow zone contouring each load cast, with the two domains still visible (Fig. 6C).

In the deformed sandy and silty sediments there are visible remnants of five lithofacies (called sublayers *a–e*) with preserved primary structures (Fig. 7A). In the lowermost part of the deformed layer, (*a*) a 10 cm-thick horizontally laminated sandy silt (lithofacies FSh) sublayer occurs, above (*b*) a massive silt (lithofacies Fm) sublayer 3–5 cm thick, followed by (*c*) a 5 cm-thick horizontally laminated silty sand (lithofacies SFh) sublayer, (*d*) a massive silt (lithofacies Fm) sublayer 3–5 cm thick, and then (*e*) a ripple cross-laminated sand (lithofacies Sr) sublayer in the uppermost part. The latter infills shallow depressions, whose depth increases from NE to SW and varies between ca. 5 cm in the NE and 20 cm in the SW.

Upper deformed layer

The finer-grained, silty upper deformed layer (Fd lithofacies) within unit B (Figs 4C, 6A, I, J) is 6 to 10 cm-thick and has a sharp base and top boundaries. In the base part, the deformed silty sediments overlie laminated fines. The lateral extension of the deformed layer is limited to the occurrence of silty sediments. In the topmost part, grain size grows gradually, changing into a thin layer of coarser-grained ripple cross-laminated sand. The most commonly occurring SSDS in the upper part of unit B are small-scale water/sediment-escape structures accompanied by flame structures, which all show a general uniform vergence, and irregularly shaped pseudonodules (Fig. 6I, J). The maximum height of single water/sediment-escape structures and flame structures reaches 2 cm, while the pseudonodules do not exceed 1 cm in diameter. The style of deformation (water/sediment-escape structures to flame structures and pseudonodule ratio) varies with the lateral extent of the deformed layer.

Interpretation

The type and frequency of SSDS within two well-defined deformed layers (lithofacies FSd and Fd) suggests the possibility of a repeatedly occurring liquefaction process. One of the first steps in seismite recognition is the indication of liquefaction features in the sediments (see Moretti, Ronchi 2011) which are relatively easily to recognize (e.g. water/sediment

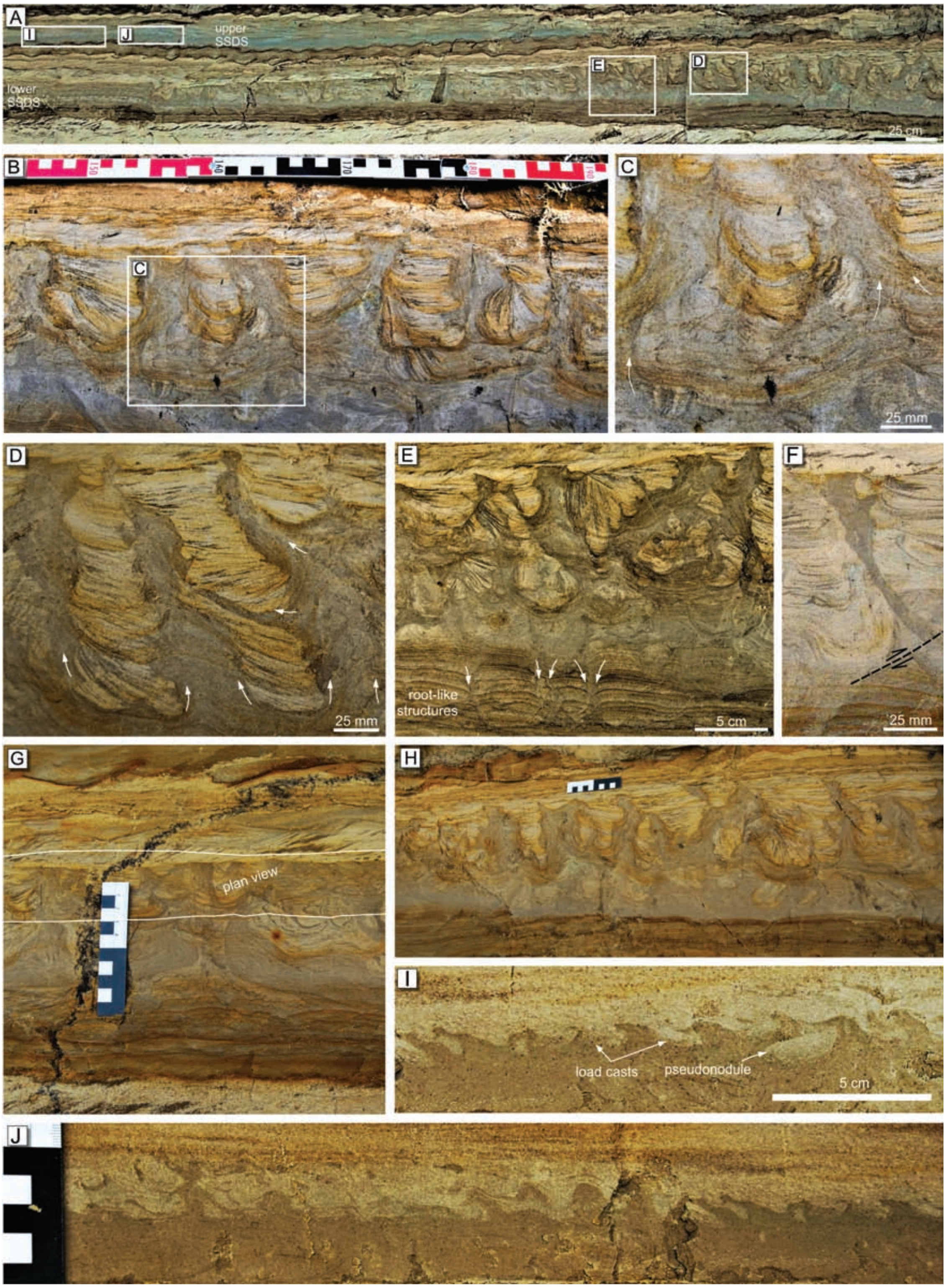

Fig. 6 Soft-sediment deformation structures within lower part of unit B in the Slinkis outcrop. **A:** Lower and upper layers with soft-sediment deformation structures within unit B. Note the regular distribution of SSDS within layer. **B:** Water/sediment-escape structures (mixed silty sand with sandy silt) injecting into ripple cross-laminated fine-grained sandy sediments. **C:** Close-up view of liquefaction features (white arrows). Note the rotated load structures. **D:** Set of narrow and slender water/sediment-escape structures intruded into overlying ripple cross-laminated sandy deposits. White arrows show relative direction of injected sediments upward movement. **E:** Water/sediment-escape structures affected lower-laying laminated sandy silt sediments (root-like structures). White arrows show relative direction of injected sediments upward movement. **F:** Water/sediment-escape structure causing bending of surrounding mixed sandy-silty sediments. **G:** Upwards water/sediment-escape structures which deformed upper-laying sublayers *b–e* (see details at Fig. 7). **H:** Two levels of load structures: lower – gentle visible, and upper – with sharp, well-visible boundaries. **I–J:** Flame structures and load casts occurred in the upper deformed layer of unit B

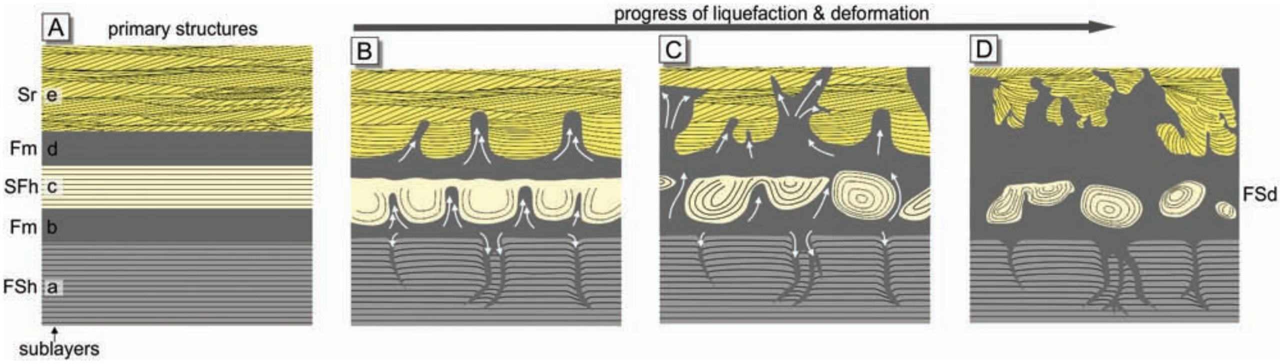

Fig. 7 Model of soft-sediment deformation structures development in the lower deformed layer of unit B in the Slinkis outcrop. **A:** Primary lithofacies (sublayers) involved in deformation process. **B–D:** Progress of liquefaction process and soft-sediment deformation structures development. See details at Fig. 4

escape-structures). The liquefaction happens shortly after deposition of the sediments, and the top boundaries of both contemporary-visible layers were palaeosurfaces during the liquefaction process. A rapid and relatively high increase of water pressure must have occurred, initiating nearly vertical, upwards movement of the fluidized sediment due to liquefaction.

Lower deformed layer

The development of SSDS in the lower deformed layer probably began with the liquefaction of two fluidized silty sublayers *b* and *d* (Fig. 7B–D). The water/sediment-escape structures in sublayer *b* are developed upwards and downwards under condition of high water pressure (Fig. 6E–G). The presence of sharp features at the topmost part of some water/sediment-escape structures (top of sublayer *e*) may suggest that they were primarily silty volcanoes, whose cones must have been eroded by water currents during the deposition of overlying ripple cross-laminated sand. The downwards injections cut the horizontally laminated sandy silt of sublayer *a* by vertical and subvertical structures and deform adjacent sediment (Fig. 6E at the lower part of the photo). The downwards injections stop at 2 mm-thick clay laminae made impermeable following impregnation of Fe^{3+}: some of the downwards vertical/subvertical injections are therefore divided into a number of smaller branches which deformed the silty laminae and created root-like structures at the base of lithofacies FSd visible today (Fig. 6E). The upper part of sublayer *a* forms one upwards water/sediment-escape structure which deformed sublayers *b–e* (Fig. 6G).

In addition, under high pressure, conditions in sublayer *b* caused the upwards injections. Some of them cut sublayers *c* and *d*. As a result of the upwards mobilization of sublayer *b,* load casts are formed (Fig. 6I, J). They are developed as a result of the sinking of the upper sublayer *c* and the upwelling of diapirs of the lower sublayer *b*, with the inner structure of load casts thus being laminated parallel to the outer shape of the form (Fig. 6I). The liquefied silty sediment (sublayer *d*) forms a second horizon of load casts, which increase in height from NE to SW and are directly connected to the thickness of the ripple cross-laminated sublayer *e*. The diapirs of silty sediment are pierced by narrow flame structures and do not cut the upper sandy rippled sublayer *e*, which remains undeformed (Fig. 6I). In all cases the main vertical upwelling diapirs form horizontal, subvertical and downward secondary injections resulting in the formation of pseudonodules (Fig. 7). The water content and pressure of the mobilised silty sediment was high, as some of load casts were tilted and rotated (Fig. 6B, C). Part of them appear to be 'sinking' in the liquidized silty sublayer *d*. The straight inner lamination observed in most load casts indicates that no such loading or sinking occurred, or at least occurred to a very limited extent (Fig. 6I).

Upper deformed layer

The SSDS in the upper deformed layer represents a classical Rayleigh-Taylor instability. The lower layer began to be liquidized and the overlying laminated fines sank underneath. Following this, the developed flame structures were re-shaped in the direction of the palaeocurrent as a result of water flowing over freshly accumulated deposits in a hydroplastic state (see Kelling, Walton 1957; Brodzikowski, Hałuszczak 1987). This process could be the reason why most flame structures show a uniform vergence.

Faults in the units A and B

Description

The third group of deformations detected in the Slinkis outcrop contain almost exclusively reverse faults (see Figs. 4B, C, E, 8A, B). Twenty-six small-scale, dip-slip reverse faults and accompanying complementary faults were observed in the sedimentary units and in the contact zone with the overloading glacial diamicton. The length of the faults varied from

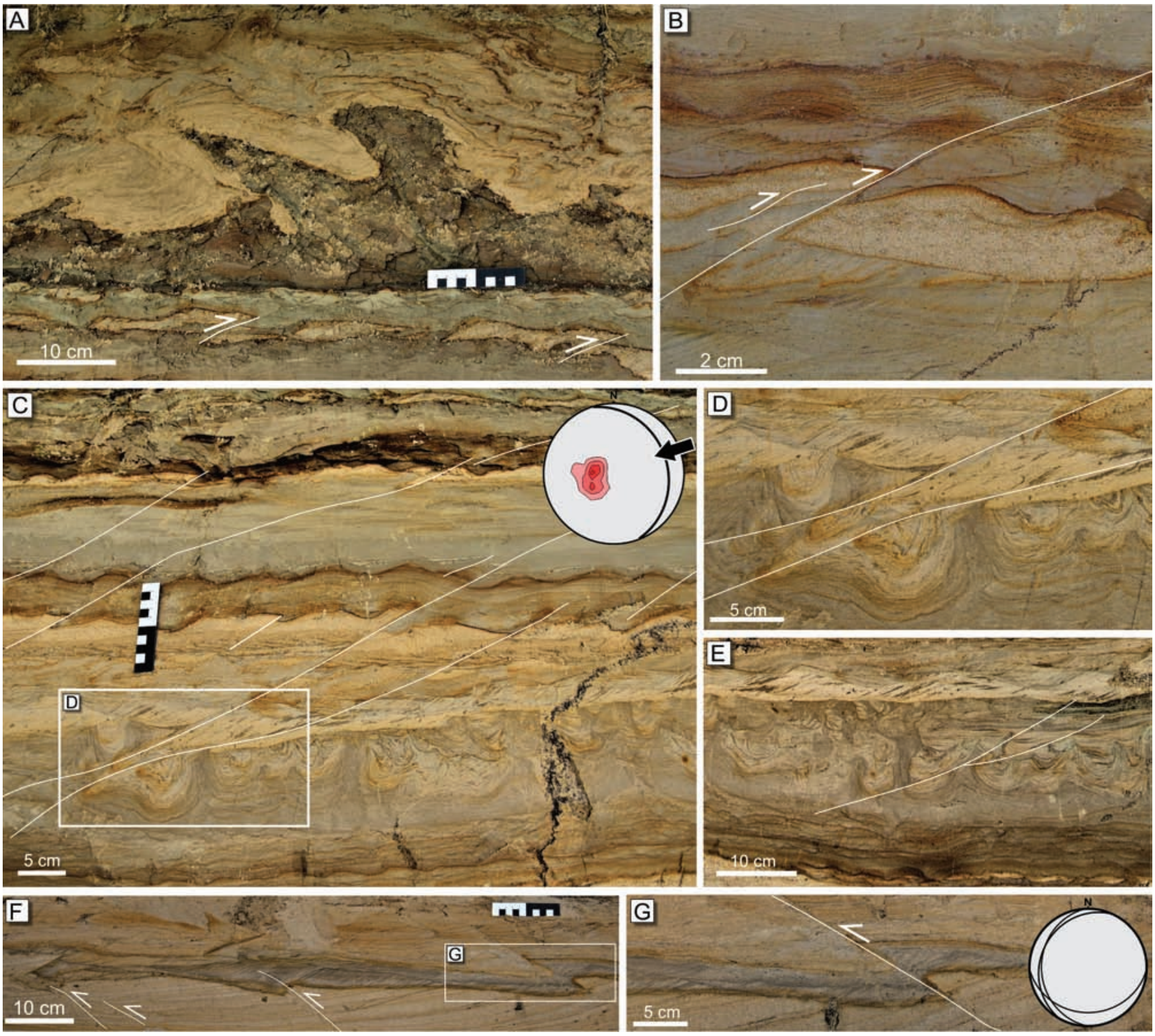

Fig. 8 Faults in units A and B in the Slinkis outcrop. **A:** Faults and folds in the upper part of unit B. **B:** Small-scale reverse faults within the upper part of unit B with stereographic projection of fault plane orientation. **C:** Low-angle reverse and listric faults cutting both units A and B of meandering river succession. **D–E:** Faults cutting and displacing soft-sediment deformation structures within unit B. **F–G:** Small-scale reverse faults within the upper part of unit A with stereographic projection of fault plane orientation

10 cm to 1.2 m, while the slip range in length from 2 to 5 cm. These low-angle faults cut and intersect individual SSDS, i.e. the loading structures and water/sediment-escape structures described in previous subchapter (Fig. 8C–E).

The longest fault, 1.2 metres in length, affects the major part of the sedimentary succession, including the lower part of unit A, i.e. reaching ice-wedge casts (see description in the subchapter above), and the sediments throughout unit B. The dip angle of some of the fault planes decrease vertically, displaying a listric-fault architecture (Fig. 8D, E).

In unit A and the lower part of unit B, 22 reverse fault planes are dipping 15–45° to N, NE and E (356–117°) with a mean orientation 343/24/NE (73/24). Moreover, four small-scale reverse faults can be observed, dipping in the opposite, westward direction. Their length is limited to 6 cm with a slip reaching 1–2 cm; two are in unit A, and two in the upper part of unit B, where they act as second-order faults with orthogonal planes to those dipping in the ENE direction. Their mean orientation is 175/20/SW (265/20).

Additionally, small-scale folds (up to 5 mm-high limbs) were detected in the contact zone between the uppermost part of unit B and glacial diamicton. The six axial planes of the folds were dipping 8–12° to the WSW-NW (255–320°).

Interpretation

The common occurrence of dominating reverse faults and their architecture clearly indicate that compressive shortening in thrust regime acted as a direct deformation mechanism. The group of four second-order reverse faults probably comprises syngenetic faults complementary to the main group, which were formed from weakened sediments that had reached failure stress.

The principal direction of the maximum compressive stress (σ_1) was ENE to WSE (from 73° azimuth); in addition, the morphology of small-scale folds and orientation of their axis indicate that the main stress ran from the NE or NNE (perpendicular to the orientation of the fold axis). This recent data is in line with earlier measurements of till fabric within the overloading till, which were obtained during the geological mapping of the area (Jusienė 2004). The till fabric shows the dominating NNE-SSW long-axes azimuth. All these aforementioned features (thrust faults planes, fold axial planes and till fabric) are generally coherent and confirm that the origin of the deformations is glaciotectonic in nature and that they were formed during the Last Glacial ice-sheet advance. The reconstructed ice front direction runs from NNE-ENE.

The wide lateral extent of faults in the sediments of both lower and upper units of meandering fluvial system, as well as their vertical range, suggest that their development was postdepositional. Within the lower part of unit B (Fig. 8B–D) faulting cut the plastic SSDS and the ice-wedge cast in unit A, suggesting that their development also occurred later.

DISCUSSION

An accurate determination of the primary trigger mechanism of sediment deformation requires a critical discussion of all possible mechanisms based on the structural and textural features of the deformation structures as well as their geological context, e.g. tectonic setting, regional stratigraphy, palaeogeography and palaeoclimatic conditions. In a relatively small Slinkis outcrop, three different trigger mechanisms were found to be responsible for the development of deformation structures, and these were linked to periglacial, seismic and glaciotectonic processes. All the identified deposits, as well as their deformation structures found in the two units are directly or indirectly linked to the Grūda=Brandenburg/=Frankfurt stadial (Guobytė, Satkūnas 2011; Marks 2015, respectively) of the Nemunas=Weichselian glaciation (MIS 2) c. 22 ka.

Periglacially induced deformation structures

The final deposition of unit A occurred about 22.4 ± 1.2 ka and 22.6 ± 1.4 ka (Fig. 4C). This deposition happens in the extraglacial zone, in front of the advancing Scandinavian Ice Sheet during the Last Glacial Maximum (Grūda stadial of the Weichselian glaciation). Hence, it is highly likely that the pra-Dubysa valley had already existed; however, the distance between the ice-sheet front and the river valley remains unknown. Between units A and B, in the meandering river succession, a sedimentation break can be seen, and ice-wedge casts were formed on the exposed part of the point bars. The presence of such epigenetic/syngenetic ice-wedge casts that directly cut the major part of unit A suggests that the study area was subject to periglacial processes. The presence of multi-stages of ice-wedge growth could suggest that the accumulation in the valley was not continuous (see Vasil'chuk 2013).

Subsequently, the fine-grained lithofacies of unit B were deposited on the floodplain of the meandering river. The time gap between the accumulation of unit A in periglacial conditions and unit B was not too long. The presence of *Botrychium, Selaginella selaginoides, Lycopodium selago* and *Betula nana* pollen in the uppermost part of unit B indicates the presence of cold climate condition (Jusienė 2004). The landscape became almost entirely forestless, with periglacial tundra type vegetation and only sparse groups of spruce and birch trees (Borisova 2005). The lack of cryostructures in unit B could result from (1) the erosion of floodplain sediments (with cryostructures) by water current (see: erosional features of the topmost part of water/sediment escape structures) or flood events and/or (2) the subaqueous conditions prevailing on the floodplain. This means that sediments were covered for most of time by a water film which does not favour the development of cryostructures (see Vasil'chuk 2013).

Seismically induced deformation structures

During floodplain deposition, the water-saturated sediments (fluidized state) were affected by at least two liquefaction processes, resulting in the deformation of floodplain sediments. As a consequence, two layers with SSDS were developed (Fig. 6A). A critical feature of the present arrangement is that the two deformed levels are interbedded between undeformed layers with similar granulometry composition. Furthermore, all SSDS are 'trapped' within two well-defined layers. This excludes periglacial processes or glaciotectonics as direct causes of these deformation structures.

The sedimentological investigations allow the relative time of the liquefaction process working in the lower deformed layer to be estimated. The erosional nature of the upper parts of some water/sediment-escape structures (Fig. 6B, E, F) indicate that liquefaction happened when sublayer *e* was a palaeosurface (see Fig. 7). As almost one metre of floodplain sediments can be observed above the lower deformed layer (i.e. the same granulometry as deformed layer), it is possible to exclude four of the six chief mechanisms causing liquefaction (Allen 2003): (1) "the sudden appearance of an agent from which coarse sediment is very rapidly deposited on a finer substrate", (2) "aseismic events in the region which raise pore-fluid pressures in confined sedimentary layers", (3) "changes in hydrostatic pressure and bed shear-stress related to the passage of progressive water waves or tsunami", and (4) "changes in pressure and shear stress on a bed resulting from the advection of large-scale turbulence". Allen (2003) also proposes "the seasonal melting of layered alluvium in periglacial regions…" as a potential cause; however, no evidence of even small thermal-contraction cracks, suggesting periglacial phenomena, was found in either deformed layer. The remaining possible trigger mechanism of liquefaction according to Allen (2003) is a "sufficiently powerful earthquake", which may be possible. In this sense, a sufficiently powerful earthquake would be one with a minimum magnitude of M=5, this being the minimum value for a seismically induced liquefaction process (Ambraseys 1988).

Glacial isostatic adjustment

The study area is located in a western part of the East European Craton, which is currently regarded as a stable continental region (stable continental core) of low seismic activity, but with a record of several historical earthquakes of light and moderate magnitudes not exceeding local magnitude M=5 (Lazauskiene *et al.* 2012). The area of the Slinkis outcrop is located between two superregional W-E trending fault zones – Šilutė–Polock (approx. 20 km to the S of the interpreted fault line) and Northern Prieglius–Birštonas fault zones. Both of these strike parallel to the present-day Nemunas River course along the eastern part of central Lithuania and perpendicular to the ice-sheet margin. They have been classified as the most prominent hazardous seismotectonic zones in Lithuania with the maximum magnitude of the possible earthquake reaching up to M = 5.5 (Lazauskienė *et al.* 2012). Some seismological studies have estimated the Northern Prieglius fault to have been activated by the M = 5 and 5.2 Kaliningrad earthquakes in 2004; their depth was located instrumentally at a depth of 16–20 km but estimated at 10–19 km by macroseismic observations of earthquake damage (Gregersen *et al.* 2007). However, recent modelling of the thrust-faulting mechanism for the Slinkis outcrop (Steffen *et al*., this issue) support the GIA interpretation only during two time periods: (1) after the Saalian glaciation until ca. 96 ka BP and (2) ca. 15 ka BP until today.

Glacial earthquakes

A sufficiently powerful earthquake could also have been induced in the study site by glacial earthquakes associated with such processes as large-scale stick-slip motion (Ekström *et al.* 2003, 2006). Such glacial earthquakes could be responsible for the liquefaction process and seismite development if their magnitudes were higher than M = 5 (*cf.* Ambraseys 1988). Nowadays stick-slip events can cause glacial earthquakes with a magnitude up to M = 5.5; however, these events are known to release their energy more slowly than tectonic earthquakes of comparable magnitude, they do not generate strong ground motion (*cf.* Ekström *et al.* 2003), and the magnitude-frequency relationship is different to that of tectonic earthquakes (Nettes, Ekström 2010). On the other hand, the Weichselian ice sheet was thicker than present-day glaciers, especially during its advance, so it would be reasonable to assume that the stick-slip motion of the ice sheet could be more violent and release energy faster than contemporary glaciers. Nettles and Ekström (2010) also indicate that the magnitude of glacial earthquakes depends on glacier thickness and bed topography. However, these claims should be verified by further geophysical modelling and experimental studies.

Glaciotectonically induced deformation structures

The glaciotectonically induced thrust faults and small-scale folds restricted to the contact zone between the sandy and silty topmost part of the meandering river succession (Fig. 4B, C, E) with overlying glacial diamicton and to sandy and silty sediments (Fig. 4B) of the distal floodplain developed later than the SSDS in unit B and ice-wedge casts in unit A. Reverse faults could be interpreted as typical deformations of glaciotectonic origin (Fig. 4). The morphology of small-scale folds and the orientation of their axis shows that the main direction of the stress ran from NE or NNE, i.e. perpendicular to the orientation of the fold axis. These findings are supported by the mean dip azimuth of thrust faults (73°, main stress direction from ENE) and coincide with the nature of the till fabric in glacial diamictons in the Slinkis outcrop, as well as with the fabric data of till in the nearby Kumečiai quarry (see Fig. 1) located a few kilometres to the south; together this data suggests that the regional relief-forming ice advance during the Weichselian was from the NNE (Jusienė 2004).

The NNE–ENE direction of the stress possibly reflected the very local ice flow directions associated with the orientation of the pra-Dubysa valley: the overall direction of ice flow across the central part of Lithuania during the first stage of the Last Glacial was from NW to SE (Gaigalas 1995).

CONCLUSIONS

The following conclusions can be drawn from this study:

• The meandering fluvial sedimentary succession in the Slinkis outcrop, including i.a. coarser-grained parts of the chute bar, point bars, compound bar and finer-grained floodplain, indicates that the meandering pra-Dubysa River existed in the Late Glacial, most probably before 22.4 ± 1.2 ka and 22.6 ± 1.4 ka. The meandering river collected sandy glaciofluvial sediments flowing from the ice sheet.

• The fluvial sediments were consecutively (1) exposed to periglacial conditions and affected by (2) liquefaction phenomena and (3) glaciotectonic processes during the Last Glacial Maximum.

• Epigenetic/syngenetic ice-wedge casts were developed in periglacial conditions on the surface of the exposed point bar in the meandering river.

• Two well-defined layers with SSDS (dominated by water/sediment-escape structures and accompanying load structures) are linked to at least two phases of liquefaction processes, which may have been triggered by seismic shock derived from a glacial isostatic earthquake or glacial earthquake.

• Contractional deformations, such as thrust faults, affecting the entire succession of the meandering river developed in response to glaciotectonic processes associated with the advancing Weichselian ice sheet.

ACKNOWLEDGEMENTS

We would like to thank the participants of the International Palaeoseismological Field Workshop in 2018 in Lithuania and Latvia for fruitful discussion, as well as Aldona Damušytė for the field assistance, both anonymous reviewers and Holger Steffen. The study has been financially supported by a grant for the GREBAL project (No. 2015/19/B/ST10/00661) from the National Science Centre Poland.

REFERENCES

Aber, J.S., Ber, A. 2007. Distribution of Glaciotectonism. In: Aber, J.S., Ber, A. (eds.) *Glaciotectonism. Development in Quaternary Sciences Volume 6*. Elsevier, Amsterdam, 153–190.

Aleksa, P., Bitinas, A. 2000. Glaciotectonic features in Lithuania. *Geological Quarterly 44*, 9–13.

Alfaro, P., Moretti, M., Soria, J.M. 1997. Soft-sediment deformation structures induced by earthquakes (seismites) in Pliocene lacustrine deposits (Guadix-Baza Basin, Central Betic Cordillera). *Eclogae Geologicae Helvetiae 90*, 531–540.

Allen, J.R.L. 2003. Load Structures. In: Middleton, G.V. (ed.), *Encyclopedia of sediments and sedimentary rocks*. Kluwer Academic Publishers, Dordrecht, 413–414.

Alsop, G.I., Marco, S. 2011. Soft-sediment deformation within seismogenic slumps of the Dead Sea Basin. *Journal of Structural Geology 33*, 433–457.

Ambraseys, N. 1988. Engineering seismology. *Earthquake Engineering and Structural Dynamics 17*, 1–105.

Baltrūnas, V., Švedas, K., Pukelytė, V. 2007. Periglacial conditions and deglaciation in Southern Lithuania during the Last Ice Age. In: Johansson, P., Saraala, P. (eds.) Applied Quaternary research in the central part of glaciated terrain. *Geological Survey of Finland Special Paper 46*, Espoo, 39–46.

Baltrūnas, V., Karmaza, B., Molodkov, A., Šinkūnas, P., Švedas, K., Zinkutė, R. 2010. Structure, formation and geochronology of the late Pleistocene and Holocene cover deposits in South-Eastern Lithuania. *Sedimentary Geology 231*, 85–97.

Belzyt, S., Pisarska-Jamroży, M. 2017. W jaki sposób badać sejsmity? Przegląd metod badawczych [How to study seismites? A review of research methods]. *Acta Geographica Lodziensia 106*, 171–180 [In Polish with English summary].

Bitinas, A. 2012. Implications of the palaeoseismicity of the Eastern Baltic Sea Region. *Quaternary International 1*, 52–53.

Bitinas, A., Lazauskienė, J. 2011. Implications of palaeoseismic events based on the analysis of the structures of the Quaternary deposits. *Baltica 24*, 127–130 [In Lithuanian, with English abstract].

Borisova, O.K. 2005. Vegetation and climate changes at the Eemian/Weichselian transition: new palynological data from Central Russian Plain. *Polish Geological Institute Special Papers 16,* 9–17.

Brandes, C., Polom, U., Winsemann, J. 2011. Reactivation of basement faults: interplay of ice-sheet advance, glacial lake formation and sediment loading. *Basin Research 23*, 53–64.

Brandes, C., Winsemann, J., Roskosch, J., Meinsen, J., Tsukamoto, S., Frechen, M., Tanner, D.C., Steffen, H., Wu, P. 2012. Activity along the Osning Thrust in Central Europe during the Lateglacial: Ice-sheet and lithosphere interactions. *Quaternary Science Reviews 38*, 49–62.

Brandes, C., Steffen, H., Steffen, R., Wu, P. 2015. Intraplate seismicity in northern central Europe is induced by the last glaciation. *Geology 43*, 611–614.

Brodzikowski, K., Hałuszczak, A. 1987. Flame structures and associated deformations in Quaternary glaciolacustrine and glaciodeltaic deposits: Examples from central Poland. *Geological Society of London Special Publications 29*, 279–286.

Brooks, G.R. 2018. Deglacial record of palaeoearthquakes interpreted from mass transport deposits at three lakes near Rouyn-Noranda, north-western Quebec, Canada. *Sedimentology 65*, 2439–2467.

Bryant, G., Cushman, R., Nick, K., Miall, A. 2016. Paleohydrologic controls of soft-sediment deformation in the Navajo Sandstone. *Sedimentary Geology 344*, 205–221.

Druzhinina, O., Bitinas, A., Molodkov, A., Kolesnik, T. 2017. Palaeoseismic deformations in the Eastern Baltic region (Kaliningrad District of Russia). *Estonian Journal of Earth Sciences 66,* 119–129.

Dzierżek, J., Stańczuk, D. 2006. Record and palaeogeographical implications of Pleistocene periglacial proc-

esses in the Drohiczyn Plateau, Podlasie Lowland (Eastern Poland). *Geological Quarterly 50*, 219–228.
Ekström, G., Nettles, M., Abers, G.A. 2003. Glacial earthquakes. *Science 302*, 622–624.
Ekström, G., Nettles, M., Tsai, V.C. 2006. Seasonality and increasing frequency of Greenland glacial earthquakes, *Science 311*, 1756–1758.
Evans, D.J.A., Phillips, E.R., Hiemstra, J.F., Auton, C.A., 2006. Subglacial till: formation, sedimentary characteristics and classification. *Earth-Science Reviews 78*, 115–176.
Ewertowski, M. 2009. Ice-wedge pseudomorphs and frost-cracking structures in Weichselian sediments, Central-West Poland. *Permafrost and Periglacial Processes 20*, 316–330.
French, H.M. 2007. *The Periglacial Environment*. John Wiley and Sons Ltd, Chichester, 458 pp.
French, H.M., Goździk, J.S. 1988. Pleistocene epigenetic and syngenetic frost fissures, Bełchatów, Poland. *Canadian Journal of Earth Sciences 25*, 2017–2027.
Gaigalas, A. 1995. Glacial history of Lithuania. In: Ehlers, J., Kozarski, S., Gibbard, P.L. (eds.). *Glacial Deposits in North-East Europe*. A.A. Balkema Publishers, Rotterdam, 127–135.
Gehrmann, A., Harding, Ch. 2018. Geomorphological Mapping and Spatial Analyses of an Upper Weichselian Glacitectonic Complex Based on LiDAR Data, Jasmund Peninsula (NE Rügen), Germany. *Geosciences 8*, 208–232.
Gibbard, P.L., Lewin, J. 2002. Climate and related controls on interglacial fluvial sedimentation in lowland Britain. *Sedimentary Geology 151*, 187–210.
Gladkov, A.S., Lobova, E.U., Deev, E.V., Khorzhenkov, A.M., Mazeika, J.V., Abdieva, S.V., Rogozhin, E.A., Rodkin, M.V., Fortuna, A.B., Charimov, T.A., Yudakhin, A.S. 2016. Earthquake-induced soft-sediment deformation structures in Late Pleistocene lacustrine deposits of Issyk-Kul lake (Kyrgyzstan). *Sedimentary Geology 344*, 112–122.
Goździk, J., Van Loon, A.J. 2007. The origin of a giant downward directed clastic dyke in a kame (Bełchatów mine, central Poland). *Sedimentary Geology 193*, 71–79.
Gregersen, S., Wiejacz, P., Dębski, W., Domański, B., Assinovskaya, B., Guterch, B., Mäntyniemi, P., Nikulin, V.G., Pacesa, A., Puura, V., Aronov, A.G., Aronova, T.I., Grünthal, G., Husebye, E.S., Sliaupa, S. 2007. The exceptional earthquakes in Kaliningrad district, Russia on September 21, 2004. *Physics of the Earth and Planetary Interiors 164*, 63–74.
Grollimund, B., Zoback, M.D. 2001. Did deglaciation trigger intraplate seismicity in the New Madrid seismic zone? *Geology 29*, 175–178.
Guobytė, R. 1990. Legends of the Quaternary geological and geomorphological maps at a scale of 1:50 000. Rules and methodological recommendations of the state geological investigations. Manuscript in the Archive of Lithuanian Geological Survey, Vilnius, 43 pp. [In Lithuanian].
Guobytė, R., Satkūnas, J. 2011. Pleistocene Glaciations in Lithuania. In: Ehlers, J., Gibbard, P.L., Hughes, P.D. (eds.), *Quaternary Glaciations – Extent and Chronology: A Closer Look*. Elsevier, Amsterdam, 231–246.
Hoffmann, G., Reicherter, K. 2012. Soft-sediment deformation of Late Pleistocene sediments along the southwestern coast of the Baltic Sea (NE Germany). *International Journal of Earth Sciences 101*, 351–363.
Huisink, M. 2000. Changing river styles in response to Weichselian climate changes in the Vacht valley, eastern Netherlands. *Sedimentary Geology 133*, 115–134.
Johnston, A.C. 1987. Suppression of earthquakes by large continental ice sheets. *Nature 330*, 467–469.
Jusienė, A. 2004. The first level geological mapping at a scale of 1:50 000 in the Ariogala area. Manuscript in the Archive of Lithuanian Geological Survey, Vilnius, 58 pp. [In Lithuanian].
Kelling, G., Walton, E.K. 1957. Load-cast structures: their relationship to upper surface structures and their mode of formation. *Geological Magazine 94*, 481–490.
Krzyszkowski, D. 1991. Vistulian fluviatile sedimentation near Bełchatów, central Poland. *Bulletin of the Polish Academy of Sciences, Earth Sciences 39*, 311–329.
Krzyszkowski, D. 1996. Climatic control on Quaternary fluvial sedimentation in the Kleszczów Graben, Central Poland. *Quaternary Science Reviews 15*, 315–333.
Lazauskienė, J., Pačėsa, A., Satkūnas, J. 2012. Seismotectonic and seismic hazard maps of Lithuania – recent implications of intracratonic seismicity in the Eastern Baltic Region. *Geologija 54*, 1–9.
Marks, L. 2015. Last deglaciation of northern continental Europe. *Cuadernos de Investigacion Geografica 41*, 279–293.
Miall, A.D. 1977. A review of braided river depositional environment. *Earth Science Reviews 13*, 1–62.
Moretti, M., Ronchi, A. 2011. Liquefaction features interpreted as seismites in the Pleistocene fluvio-lacustrine deposits of the Neuquén Basin (Northern Patagonia). *Sedimentary Geology 235*, 200–209.
Muir-Wood, R. 2000.Deglaciation seismotectonics: a principal influence on intraplate seismogenesis at high latitudes. *Quaternary Science Reviews 19*, 1399–1411.
Nettles, M., Ekström, G. 2010. Glacial earthquakes in Greenland and Antarctica. *Annual Reviews of Earth Planetary Sciences 38*, 467–491.
Pedersen, S.A.S. 2014. Architecture of Glaciotectonic Complexes. *Geosciences 4*, 269–296.
Phillips, E.R., Evans, D.J.A., Van der Meer, J.J.M., Lee, J.R. 2018. Microscale evidence of liquefaction and its potential triggers during soft-bed deformation within subglacial traction tills. *Quaternary Science Reviews 181*, 123–143.
Pisarska-Jamroży, M. 2013. Varves and megavarves in the Eberswalde Valley (NE Germany) – a key for the interpretation of glaciolimnic processes. *Sedimentary Geology 29*, 84–96.
Pisarska-Jamroży, M., Zieliński, T. 2012. Specific erosional and depositional processes in a Pleistocene sub-

glacial tunnel in the Wielkopolska region, Poland. *Geografiska Annaler 94A*, 429–443.
Pisarska-Jamroży, M., Belzyt, S., Börner, A., Hoffmann, G., Hüneke, H., Kenzler, M., Obst, K., Rother, H., Van Loon, A.J. 2018. Evidence from seismites for glacio-isostatically induced crustal faulting in front of an advancing land-ice mass (Rügen Island, SW Baltic Sea). *Tectonophysics 745*, 338–348.
Pisarska-Jamroży, M., Woźniak, P.P. 2019. Debris flow and glacioisostatic-induced soft-sediment deformation structures in a Pleistocene glaciolacustrine fan: The southern Baltic Sea coast, Poland. *Geomorphology 326*, 225–238.
Pisarska-Jamroży, M., Van Loon, A.J., Roman, M., Mleczak, M. 2019. Enigmatic gravity-flow deposits at Ujście (western Poland), triggered by earthquakes (as evidenced by seismites) caused by Saalian glacioisostatic crustal rebound. *Geomorphology 326*, 239–251.
Podolskiy, E.A., Walter, F. 2016. Cryoseismology. *Reviews of Geophysics 54*, 708–758.
Rana, N., Sati, S.P., Sundriyal, Y., Juyal N. 2016. Genesis and implication of soft-sediment deformation structures in high-energy fluvial deposits of the Alaknanda Valley, Garhwal Himalaya, India. *Sedimentary Geology 344*, 263–276.
Ruczyńska-Szejnach, H., Trzciński, J. 2009. Soft lodgement till deposition and syndepositional deformation, Anielinek, the Polish Lowlands. *Canadian Journal of Earth Sciences 46*, 67–82.
Schwan, J., Van Loon, A.J. 1979. Structural and sedimentological characteristics of a Weichselian kame terrace at Sönderby Klint, Funen, Denmark. *Geologie en Mijnbouw 58*, 305–319.
Steffen, H., Wu, P. 2011. Glacial isostatic adjustment in Fennoscandia – a review of data and modelling. *Journal of Geodynamics 52*, 169–204.
Steffen, R., Wu, P., Steffen, H., Eaton, D.W. 2014. The effect of earth rheology and ice-sheet size on fault slip and magnitude of postglacial earthquakes. *Earth and Planetary Science Letters 388,* 71–80.
Steffen, H., Steffen, R., Tarasov, L. 2019. Modelling of glacially-induced stress changes in Latvia, Lithuania and the Kaliningrad District of Russia. *Baltica* (this issue).
Stewart, I.S., Sauber, J., Rose, J. 2000. Glacio-seismotectonics: ice sheets, crustal deformation and seismicity. *Quaternary Science Reviews 19*, 1367–1389.
Van Loon, A.J. 2009. Soft-sediment deformation structures in siliciclastic sediments : an overview. *Geologos 15*, 3–55.
Van Loon, A.J., Brodzikowski, K. 1987. Problems and progress in the research on soft-sediment deformations. *Sedimentary Geology 50*, 167–193.
Van Loon, A.J., Pisarska-Jamroży, M. 2014. Sedimentological evidence of Pleistocene earthquakes in NW Poland induced by glacio-isostatic rebound. *Sedimentary Geology 300*, 1–10.
Van Loon, A.J., Pisarska-Jamroży, M., Nartišs, M., Krievāns, M., Soms, J. 2016. Seismites resulting from high-frequency, high-magnitude earthquakes in Latvia caused by Late Glacial glacio-isostatic uplift. *Journal of Palaeogeography 5*, 363–380.
Vandenberghe, J. 2008. The fluvial cycle at cold-warm-cold transitions in low land regions: A refinement of theory. *Geomorphology 98*, 275–284.
Vandenberghe, J., Kasse, C., Bohnke, S., Kozarski, S. 1994. Climate-related river activity at the Weichselian-Holocene transition: a comparative study of the Warta and Maas rivers. *Terra Nova 6*, 478–485.
Vasil'chuk, Y. 2013. Syngenetic Ice Wedges: Cyclical Formation, Radiocarbon Age and Stable Isotope Records. Monograph Synopsis. *Permafrost and Periglacial Processes 24*, 82–93.
Weckwerth, P., Pisarska-Jamroży, M. 2015. Periglacial and fluvial factors controlling the sedimentation of Pleistocene breccia in NW Poland. *Geografiska Annaler 97A,* 415–430.
Woronko, B., Belzyt, S., Bujak, Ł., Pisarska-Jamroży, M. 2018. Glaciotectonically deformed glaciofluvial sediments with ruptured pebbles (the Koczery study site, E Poland). *Bulletin of the Geological Society of Finland 90*, 145–159.
Zieliński, T. 2014. *Sedymentologia. Osady rzek i jezior* [Sedimentology. Lacustrine and fluvial deposits]. UAM Press, Poznań, 594 pp. [in Polish].
Zieliński, T., Pisarska-Jamroży, M. 2012. Jakie cechy litologiczne osadów warto kodować, a jakie nie? [Which features of deposits should be included in a code and which not?] *Przegląd Geologiczny 60*, 387–397 [In Polish with English abstract].
Zieliński, T., Terpiłowski, S., Zieliński, P., Pidek, I.A., Godlewska, A., Czubla, P. 2016. What was an interglacial river like? Sedimentological investigation of Holsteinian fluvial deposits in eastern Poland. *Geological Quarterly 60*, 149–166.